

# MFHI: Taking Modality-free Human Identification as Zero-shot Learning

Zhizhe Liu, Xingxing Zhang, Zhenfeng Zhu\*, Shuai Zheng, Yao Zhao, *Senior Member, IEEE*, and Jian Cheng

arXiv:2010.00975v2 [cs.CV] 30 Dec 2021

**Abstract**—Human identification is an important topic in event detection, person tracking, and public security. There have been numerous methods proposed for human identification, such as face identification, person re-identification, and gait identification. Typically, existing methods predominantly classify a queried image to a specific identity in an image gallery set (I2I). This is seriously limited for the scenario where only a textual description of the query or an attribute gallery set is available in a wide range of video surveillance applications (A2I or I2A). However, very few efforts have been devoted towards modality-free identification, i.e., identifying a query in a gallery set in a scalable way. In this work, we take an initial attempt, and formulate such a novel Modality-Free Human Identification (named MFHI) task as a generic zero-shot learning model in a scalable way. Meanwhile, it is capable of bridging the visual and semantic modalities by learning a discriminative prototype of each identity. In addition, the semantics-guided spatial attention is enforced on visual modality to obtain interpretable representations with both high global category-level and local attribute-level discrimination. Finally, we design and conduct an extensive group of experiments on two common challenging identification tasks, including face identification and person re-identification, demonstrating that our method outperforms a wide variety of state-of-the-art methods on modality-free human identification.

**Index Terms**—Human identification, zero-shot learning, prototype learning, deep learning

## I. INTRODUCTION

GENERALLY, human identification aims to verify the identity of a person based on one or more biometric features, e.g., face [1], gait [2], and person image [3]. It has been widely used in various areas such as stations, schools, and companies, since human identification is crucially important in surveillance [4], activity analysis [5], and person search [3]. Especially, as two typical representatives of human identification, face identification and person re-identification (re-ID) play a key role in such an important topic, and have

This work was supported in part by Science and Technology Innovation 2030 – New Generation Artificial Intelligence Major Project under Grant 2018AAA0102101, in part by the National Natural Science Foundation of China under Grant No. 61976018.

Z. Liu, Z. Zhu, S. Zheng and Y. Zhao are with the Institute of Information Science, Beijing Jiaotong University, Beijing 100044, China, and also with the Beijing Key Laboratory of Advanced Information Science and Network Technology, Beijing Jiaotong University, Beijing 100044, China (E-mail: zhliu@bjtu.edu.cn; zhfzhu@bjtu.edu.cn; zsl997@bjtu.edu.cn; yzhao@bjtu.edu.cn). (*Corresponding author: Zhenfeng Zhu.*)

X. Zhang is with the Department of Computer Science and Technology, Tsinghua University, Beijing 100084, China. E-mail: xxzhang2020@mail.tsinghua.edu.cn.

Jian Cheng is with the National Laboratory of Pattern Recognition, Institute of Automation, Chinese Academy of Sciences, Beijing, China (E-mail: jcheng@nlpr.ia.ac.cn).

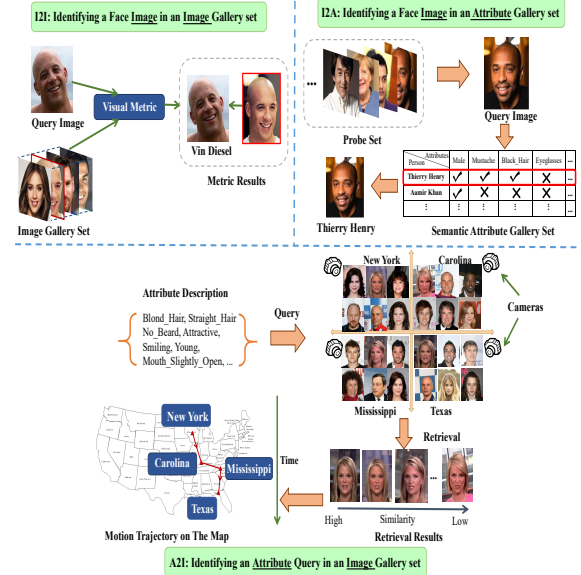


Fig. 1. The illustration of modality-free face identification, including I2I, I2A, and A2I three scenarios.

received extensive attention and success recently. In this work, we focus on these two challenging identification tasks.

In recent years, owing to significant advances in deep learning and discriminative learning approaches [1], convolutional neural networks (CNN) have increased the face identification to an unprecedented level. Generally, a face identification method involves a training set, a gallery set, and a probe set, where the gallery set of target identity must be collected before classifying a query from a probe set. There are open-set and close-set two settings in face identification task. For the close-set, the queried identity must appear in the training set, while for the open-set, it generally never appears. This is very important and popular since collecting sufficient training data for all possible identities would be very difficult. Obviously, face identification in open-set is more suitable for complex scenarios in daily life, and has been widely explored [1]. Thus, we mainly study open-set case in this work.

Similar to face identification, re-ID also obtains significant improvements with the help of rich deep visual features, and has been widely used in many situations such as long-term multi-camera tracking [4] and activity analysis [5]. Recently, due to the increasing number of surveillance cameras, a large amount of raw video data is continually accumulated every day. Thus, re-ID becomes more challenging and essential in real-world applications. Most existing re-ID methods focus on image queries (probe set) [3], and aim to retrieve the images with the same identity to the queried image from the

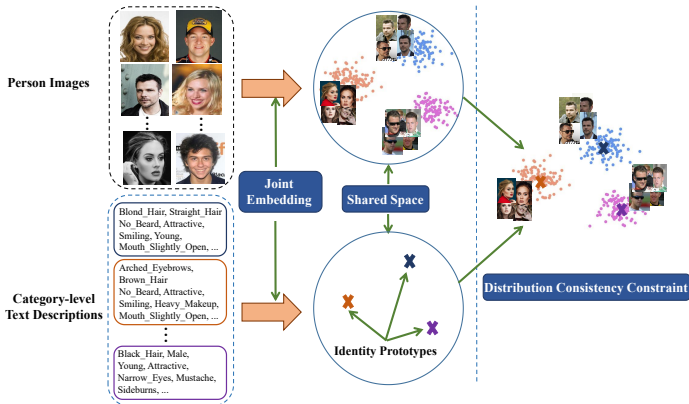


Fig. 2. The illustration of joint embedding learning in modality-free identification. For example, images and texts are embedded into a shared space, and the distributions of two modalities are consistent in the shared space.

gallery set. Generally, given a queried image, these methods calculate pairwise visual similarity scores between the queried image and every gallery image in the gallery set, and then treat the gallery images with the higher similarity scores as possible matches. Specially, it is worth noticing that the person identities in training and gallery sets are also disjoint in re-ID.

However, existing face identification and re-ID tasks predominantly focus on how to accurately classify a queried image to a specific identity in an image gallery set. Actually, in many practical scenarios, only a textual description of the query, instead of an image, is available. Likewise, only a gallery set that collects all textual descriptions of target identities, but not images, is provided. This is closely related to a wide range of video surveillance applications. Taking face identification as an example, as shown in Fig. 1, based on an pre-collected image gallery set, the first case aims to verify the identity of the query image. The goal of the second case is to classify a queried face image to a specific identity in an attribute gallery set, since the corresponding image gallery set (i.e., visual information) cannot be provided for privacy protection. The third case is to retrieve images with the same identity from an image gallery set, if a queried face attribute description is given. We name face identification in all these scenarios as **modality-free face identification**. For example, given a list of textual descriptions from witnesses, i.e., criminal portrait, we aim to perform face identification from a provided image gallery set, and further obtain the motion trajectory of criminal on the map. In fact, the current human identification methods mainly focus on the independent Image→Image and Attribute→Image identification and have obtained impressive results. However, such independent models obviously won't allow flexible transfer between different recognition tasks such as Image→Image and Attribute→Image. Meanwhile, in realistic identification scenarios, we usually require the model with strong robustness and generalizability to address various identification tasks. From a practical point of view, it means that the ability to transfer between tasks is necessary when developing a flexible human identification model.

Furthermore, considering that only a small ration of identities can be used for model training in open-set setting, we take an initial attempt, and formulate such a modality-free

human identification task as a zero-shot learning (ZSL) model. Generally, ZSL [6] aims to classify objects which may not have any training samples. Although ZSL has obtained great progress [7], existing ZSL methods are suboptimal for our problem. *First*, conventional ZSL setting usually assigns a label for a queried image within a small scale categories, while human identification is actually a more challenging and larger scale ZSL problem. *Second*, existing ZSL setting is with both low inter-class similarity and small intra-class variation, while it is contrary for human identification problem. This results in the image features learned by existing ZSL methods would be indiscriminate [6], [8] for such a challenging identification task. *Third*, existing ZSL methods only consider classifying a queried image to a category in an attribute gallery set [9], i.e., the second case in Fig. 1. They cannot be directly extended for modality-free human identification.

Motivated by the above observations, in this work, we aim to formulate such a modality-free human identification task as a **generic** ZSL model. Concretely, inspired by ArcFace for face identification in [1], we also introduce an additive angular margin in our model for high global category-level discrimination in large-scale category scenarios. It actually has a clear geometric interpretation due to its exact correspondence to geodesic distance on a hypersphere. Moreover, to maximize the human identity separability, the local attribute-level discrimination is additionally considered in MFHI by learning an attribute-driven spatial attention. It is capable of capturing the distribution inconsistency between identities, thus enhancing the discriminative power of visual features. Finally, for modality-free human identification, we innovatively bridge the visual and semantic modalities, i.e., images and texts, by learning a shared space as shown in Fig. 2. It should be noticed that some previous cross-modality matching methods typically focus on point-to-point distribution consistency through paired image-text sample (e.g., ranking loss based methods [3], [10]). Although these methods have achieved impressive results in image-text matching, they cannot effectively address human identification tasks due to the presence of many unseen identities in realistic scenarios. However, our MFHI aims to bridge visual and semantic modalities by prototype learning and maximize the distribution consistency between the visual embedding and identity prototypes.

We emphasize our **contributions** in four aspects:

- To the best of our knowledge, our work describes the first algorithmic framework for the modality-free human identification task.
- We formulate such a task as a generic zero-shot learning model, which can bridge the visual and semantic modalities by prototype learning.
- To obtain highly discriminative features in both global category-level and local attribute-level, a semantics-guided attention map is further learned in our model, thus leading to more reliable and interpretable identification.
- Extensive experiments demonstrate our method could achieve competitive results on modality-free identification, including face identification task and re-ID task.

TABLE I  
KEY NOTATIONS.

Notations	Descriptions
$Y^s, Y^u$	Set of seen identities and set of unseen identities, respectively
$\mathbf{A}^{tr/te}, \hat{\mathbf{A}}^{tr/te}$	Set of image-level and category-level attribute descriptions about training/testing identities, respectively
$\mathbf{X}^{tr}, \mathbf{X}^{te}, \mathbf{X}^q$	Set of training images, set of testing images, and set of query images, respectively
$K, L$	Number of seen identities and unseen identities, respectively
$\mathbf{x}_i^{tr}, \mathbf{y}_i^{tr}$	The $i$ -th labeled training image: $\mathbf{x}_i^{tr} \in \mathbf{X}^{tr}, \mathbf{y}_i^{tr} \in Y^s$
$\mathbf{x}_i^{te}$	The $i$ -th unlabeled testing image: $\mathbf{x}_i^{te} \in \mathbf{X}^{te}$
$\mathbf{x}_i^q$	The $i$ -th query image: $\mathbf{x}_i^q \in \mathbf{X}^q$
$\mathbf{a}_i^{tr/te}, \hat{\mathbf{a}}_j^{tr/te}$	The attribute vector of the $i$ -th training/testing image, and the attribute vector of the $j$ -th training/testing identity
$f_{12A}(\cdot)$	The function of classifying an image by attribute descriptions
$f_{A2I}(\cdot)$	The function of retrieving images with the same identity as an attribute query
$f_{I2I}(\cdot)$	The function of predicting the correct label for an image query

## II. RELATED WORK

### A. Human Identification

**Face Identification.** From the view of designing the loss functions, existing face identification in open-set methods can be divided into two categories. The first group, such as softmax based methods [11], views each identity as a category, and then trains a multi-class classifier to classify different identities. The other group directly learns an embedding, such as [12] that used the triplet loss to separate the positive pair (i.e., two images with the same identity) from the negative by a distance margin. To further enhance the discriminability of visual features, there also appear some variants of the softmax loss recently [1], [13]. For example, Deng et al. [1] proposed an additive angular margin loss to directly optimize the geodesic distance margin by virtue of the exact correspondence between the angle and arc in the normalized hypersphere. This can help to obtain highly discriminative features for face identification. Benefiting from the large-scale training data and the elaborate CNN, both the softmax-loss-based and the triplet-loss-based methods can achieve excellent performances on face identification. However, all these methods only consider an image modality, which is seriously limited for the scenarios where only a textual query or an attribute gallery set is available.

**Person Re-identification.** Most re-ID researches take images as probes (i.e., queries) and then retrieve the corresponding person images from a pre-collected gallery set [3]. However, due to the limitations of realistic scenarios, we are not always able to obtain the query images. Recently, a number of researches focus on language-based person re-ID [14], [15], [16], [17]. These language-based re-ID methods can be divided into two categories. The first category [14], [16] aims to learn a more discriminative visual representation with the help of attributes. For example, a multi-task person re-id network was proposed in [14] to learn a Re-ID embedding and at the same time to predict the pedestrian attributes. Tianrui Chai *et al.* [16] proposed an Attribute Salient Region Enhance (ASRE) module to learn a better separation of the pedestrian from background. The second category [15], [17] aims to retrieve the matched person images when only a textual description is given, such as in [15], an instance loss for instance-level image-text matching was proposed based on the assumption that each image/text group is distinct.

However, there are still existing additional challenges in various application scenarios. First, existing methods are

not flexible, since they can only solve queries with single text or image modality, so it is difficult to extend them to modality-free queries. Second, it is expensive to collect rich natural language descriptions for each person image. Third, some methods based on natural language descriptions are discommodious because they usually need to model rich and complex sentence syntax. In contrast, collecting short attribute descriptions is very simple, and it also retains most of the semantic information. Specially, in realistic scenarios, short attribute descriptions make it easier for witnesses to paint a portrait of the criminal, and if the search results do not meet expectations, we can quickly and accurately modify the descriptions to refine the search results.

### B. Zero-Shot Learning

Existing ZSL models consist of transductive [18] and inductive [6], [8], [7], [19] two settings, with the former employing the information about the unseen domain during model training, and the latter not. Specially, the transductive setting in ZSL is proposed to alleviate the domain shift problem between seen and unseen domains. Despite the transductive ZSL approaches have been shown to improve the generalizability of the model in the unseen domain, it is not always feasible in realistic scenarios, e.g., open-set setting in face identification. Thus, we take an inductive setting in this work.

From the view of constructing the visual-semantic interactions, existing inductive ZSL methods can be divided into four categories. The first group focuses on learning a projection function from the visual to the semantic space with a linear [8] or a non-linear model [7]. In contrast, the second group learns a projection function from the semantic to the visual space [6], [20]. In [20], Chen *et al.* developed a feature refinement (FR) module that incorporates semantic→visual mapping into a unified generative model to refine the visual features of seen and unseen class samples. Combining the above methods, the third group employed an encoder-decoder paradigm with the visual or class prototype reconstruction constraint [8]. For example, by utilizing the structure of the space spanned by the attributes, PSR [8] learned an encoder-decoder multilayer perceptron (MLP) model to preserve the structure of the semantic space in the visual space. The last group learns an intermediate space, where both the visual and semantic space are projected to [21].

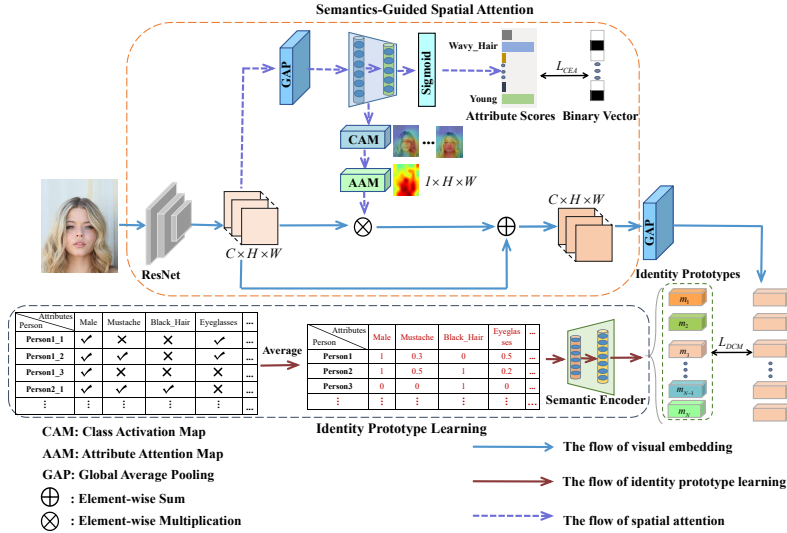


Fig. 3. The overall architecture of our proposed generic zero-shot learning model for modality-free human identification.

### III. METHODOLOGY

In this section, we first set up our modality-free human identification problem, and then formulate it as a generic zero-shot learning model.

#### A. MFHI: Problem Definition

The key notations used throughout this paper are summarized in Table I. Let  $Y^u = \{u_1, \dots, u_L\}$  denote the unseen target identity set, and these  $L$  identities do not have any labeled training samples. However, we have an attribute vector set  $\mathbf{A}^{te} = [\mathbf{a}_1^{te}, \dots, \mathbf{a}_T^{te}]$  (i.e., an attribute gallery set), where  $\mathbf{a}_i^{te} \in \mathbb{R}^Q$  is a binary vector. It involves the textual descriptions of  $T$  images about the  $L$  identities. Then we can get the category-level attribute vector set  $\hat{\mathbf{A}}^{te} = [\hat{\mathbf{a}}_1^{te}, \dots, \hat{\mathbf{a}}_L^{te}]$  for these  $L$  identities by averaging the image-level attribute vectors of each identity. Similarly, an image gallery set is denoted as  $\mathbf{X}^{te} = [\mathbf{x}_1^{te}, \dots, \mathbf{x}_T^{te}]$ , which represents  $T$  images belonging to the  $L$  identities. In addition, an image probe set consisting of  $P$  queried images about the  $L$  identities is represented as  $\mathbf{X}^q = [\mathbf{x}_1^q, \dots, \mathbf{x}_P^q]$ . During the testing phase, we denote (i) **Image**→**Attribute (I2A)** as the task that assigns a correct label for a testing image of the target identity when only an attribute gallery set is available. Therefore, we need to learn a function  $f_{I2A}(x, \hat{\mathbf{A}}^{te})$  to predict the label  $y$  of an image  $x$  within  $L$  different identities. (ii) While a queried textual description  $\mathbf{a}$  is provided, **Attribute**→**Image (A2I)** focuses on retrieving the images with the same identity from an image gallery set. Thus, a retrieval function  $f_{A2I}(\mathbf{a}, \mathbf{X}^{te})$  is required. (iii) As a common setup in conventional human identification, **Image**→**Image (I2I)** aims to verify the label for a queried image  $x$  from a probe set based on an image gallery set. For this end, we need to learn a prediction function  $f_{I2I}(x, \mathbf{X}^{te})$ .

To flexibly and effectively tackle the above three tasks, as the previous human identification work [1], we also introduce a training set  $\mathcal{D}^{tr} = \langle \mathcal{X}^{tr}, \mathcal{Y}^{tr} \rangle$  that contains another  $K$  identities, where  $\mathcal{X}^{tr}$  and  $\mathcal{Y}^{tr}$  denote the sets of training images and labels respectively. Let  $Y^s = \{s_1, \dots, s_K\}$  denote the set of these  $K$  identities. Likewise,  $\mathbf{A}^{tr} = [\mathbf{a}_1^{tr}, \dots, \mathbf{a}_S^{tr}]$

and  $\hat{\mathbf{A}}^{tr} = [\hat{\mathbf{a}}_1^{tr}, \dots, \hat{\mathbf{a}}_K^{tr}]$  represent their image- and category-level attribute vector sets respectively. It is worth noticing that, typically,  $K > L$ , and  $Y^u \cap Y^s = \emptyset$ . This is just our open-set modality-free human identification problem.

#### B. MFHI: Overall Framework

The overall framework of our MFHI is shown in Fig. 3, which mainly includes three flows (visual embedding flow, spatial attention flow, and prototype learning flow). Note that it is a unified architecture that can be flexibly applied to learn the three kinds of prediction functions, i.e.,  $f_{I2A}(\cdot)$ ,  $f_{A2I}(\cdot)$ , and  $f_{I2I}(\cdot)$  in all three scenarios. Concretely, for any input image  $x$ , the *visual embedding flow* first obtains a visual feature map  $F = \Psi(x) \in \mathbb{R}^{C \times H \times W}$ . Afterwards, the feature map  $F$  is fed into the *spatial attention flow* to generate an attention map. Specially, in this flow, we first infer the attribute scores which help to gain the confidence about each attribute. Then, for each attribute, we build the class activate map which can localize the class-sensitive activation region. Relying on the attribute scores, we select the *Top-D* attribute class activation maps of the image, since the attentive regions captured in these activation maps have important discriminability. After that, the attribute attention map  $M_a \in \mathbb{R}^{1 \times H \times W}$  is generated by maximum operation to these activation maps. Consequently, the new feature map  $F' = (F \otimes M_a) \oplus F$  is updated by enforcing such a semantics-guided attention map, where  $\otimes$  and  $\oplus$  represent element-wise multiplication and element-wise sum operations respectively. Thus, we can get the more discriminative visual feature of the input image via global average pooling operation to  $F'$ . Furthermore, a prototype learning flow is introduced to learn an identity prototype from its category-level textual description via a MLP. As a result, we can perform MFHI with modality-free property, since the visual and semantic spaces can be bridged seamlessly by the three flows. Once the visual feature of an image and the class prototype of a target identity are learned, we can conduct modality-free human identification.

*C. MFHI: Semantics-Guided Spatial Attention (SGSA)*

Existing ZSL methods mainly focus on extracting global visual feature from an image. This is usually ineffective for large-scale human identification, where there exist small inter-class and large intra-class distances. To maximize inter-class separability, some methods [22], [23], [24] proposed semantic-guided attention to capture local discriminative regions. Specially, inspired by AAnet [22], we propose to learn a semantics-guided spatial attention (SGSA) map to capture the most discriminative local attribute regions. Meanwhile, such an attention can lead to more reliable and interpretable identification. It is worth noting that our SGSA is greatly different from AAnet especially in network complexity and input. Specifically, our SGSA consists of an attribute prediction module (APM) that can individually predict each attribute and an attribute attention module (AAM). Referring to [25], AAM can produce a class activation map for each individual attribute by utilizing the weight of attribute classifier in APM. Then, according to the predicted attribute scores of an image, the semantics-guided spatial attention map is generated by aggregating the *Top-D* class activation maps.

**- Attribute Prediction Module (APM)**

As shown in Fig. 3, the feature map with the size of  $C \times H \times W$  is first down-sampled to  $C \times 1 \times 1$  by global average pooling (GAP) operation, which helps find all discriminative regions in an image. We reshape it to  $\mathbb{R}^{C \times 1}$  to get the visual feature vector. Then, we can predict the attribute score vector  $p \in \mathbb{R}^Q$  based on the locally discriminatively enhanced visual features. After that,  $p$  is normalized by a sigmoid activation layer, and finally we can get the confidence score of each attribute.

**- Attribute Attention Module (AAM)**

To obtain the representation with local attribute-level discrimination, we first get the class activation map for each individual attribute. Let  $\mathbf{W}_{apm} \in \mathbb{R}^{Q \times C}$  represent the weight matrix of attribute classifier in APM, and  $w_{ij}$  is the  $j$ -th column of  $i$ -th row in  $\mathbf{W}_{apm}$ . Then we define  $CAM_i$  as the class activation map of the  $i$ -th attribute, where the element in spatial position  $(a, b)$  is computed as follows:

$$CAM_i(a, b) = \sum_{j=1}^C w_{ij} F_j(a, b) \quad (1)$$

where  $a \in [1, H]$  and  $b \in [1, W]$ .  $F_j$  represents the  $j$ -th channel of feature map  $F$ .

Meanwhile, we descendingly sort the attribute scores  $p$  obtained in APM. Then, we select the *Top-D* attributes with the highest scores, since these local regions normally have significant representation ability. After that, we combine the CAMs of these attributes by maximum operation to generate the spatial attention map  $M_a \in \mathbb{R}^{1 \times H \times W}$ . The new feature map with both global category-level and the local attribute-level discrimination  $F' \in \mathbb{R}^{C \times H \times W}$  is generated by  $M_a$  as:

$$F' = (F \otimes M_a) \oplus F \quad (2)$$

Finally, we can get the final visual feature  $v \in \mathbb{R}^{C \times 1}$  by global average pooling operation on  $F'$ , thus leading to more reliable and interpretable identification.

*D. MFHI: Prototype Learning Module (PLM)*

Generally, there often exist noises in a list of textual descriptions of one target identity. To address this problem, we first average them to obtain a category-level attribute vector  $\hat{a}_j$ . Moreover, the fundamental challenge in MFHI actually lies in the heterogeneity of different modalities (e.g., images and texts). For this end, a shared space is learned to bridge the visual and semantic spaces. Specifically, we learn an identity prototype  $m_j$  from the category-level attribute vector  $\hat{a}_j$  with a MLP, which is defined as  $m_j = \Phi(\hat{a}_j)$ , where the dimension of the identity prototype is equal to the visual feature. Specially, for **I2I** task, since both probe set and gallery set are composed of images, the identity prototypes are replaced by the weight of a fully connected layer as in [1], and a row of the weight represents an identity prototype. This is mainly due to the fact that during the testing phase, no additional semantic descriptions are available in **I2I** task for generating identity prototypes, while the PLM based on semantic descriptions during the training phase will bring the semantic gap problem between visual and textual modalities, thus learning low-quality visual features. Finally, in order to improve the discrimination of the identity prototypes, we constrain the distribution consistency of textual prototypes and visual features by enforcing an angular margin loss as in [1].

*E. MFHI: Loss Functions*

It has been proved that episodic training can effectively mitigate the sample distribution gap between the seen and unseen classes [19], i.e., the identities in training set and gallery set. Thus, we build a series of zero-shot tasks in training set as follows by simulating the target test task for episodic training:

$$\left\{ \left\langle \mathcal{X}_1^{tr}, \hat{\mathbf{A}}_1^{tr}, \mathbf{A}_1^{tr}, \mathcal{Y}_1^{tr} \right\rangle, \dots, \left\langle \mathcal{X}_n^{tr}, \hat{\mathbf{A}}_n^{tr}, \mathbf{A}_n^{tr}, \mathcal{Y}_n^{tr} \right\rangle \right\} \quad (3)$$

In this setup, the objective of our MFHI is defined as:

$$\Pi = \arg \min_{\Theta} \sum_{i=1}^n \sum_{\{x, y\} \in \{\mathcal{X}_i^{tr}, \mathcal{Y}_i^{tr}\}} \mathcal{L}(\Theta; x, \hat{\mathbf{A}}_i^{tr}, \mathbf{A}_i^{tr}, y) \quad (4)$$

where  $\Theta$  denotes the parameter set in visual embedding, spatial attention, and prototype learning flows.

To effectively and accurately recognize any queried sample, we design two modules which can achieve two goals of: (i) Minimizing the classification error of each individual attribute (CEA); (ii) Maximizing the distribution consistency between different modalities via learned identity prototypes (DCM). Based on the above two objectives, we can decompose the objective in Eq. (4) into two functions as

$$\mathcal{L}(x, \hat{\mathbf{A}}_i^{tr}, \mathbf{A}_i^{tr}, y) \triangleq \mathcal{L}_{CEA}(x, \mathbf{A}_i^{tr}, y) + \mathcal{L}_{DCM}(x, \hat{\mathbf{A}}_i^{tr}, y)$$

**Classification Error of Attributes (CEA).** To make the class activation map accurately localize the sensitive region for each individual attribute, we need effectively predict each

individual attribute for the input image. For this end, we can minimize the classification error in the attribute level as:

$$\mathcal{L}_{\text{CEA}}(x, \mathbf{A}_i^{tr}, y) = \sum_{j=1}^Q -(r_j \log p_j + (1 - r_j) \log(1 - p_j)) \quad (5)$$

where  $r_j = 1$  if the image possesses  $j$ -th attribute and 0 otherwise.  $p_j$  is the predicted score of  $j$ -th attribute.

**Distribution Consistency between Modalities (DCM).** Suppose there exist  $N$  identities  $Y_i^s = \{s_{i1}, \dots, s_{iN}\}$  in the  $i$ -th task  $\langle \mathcal{X}_i^{tr}, \hat{\mathbf{A}}_i^{tr}, \mathbf{A}_i^{tr}, \mathcal{Y}_i^{tr} \rangle$ . Based on the category-level textual descriptions, we first obtain the prototypes of all identities in this task, represented as  $M = \{m_1, \dots, m_N\}$ . Once the identity prototype set  $M$  and the visual feature  $v$  of the input image are obtained, we then normalize them with  $\ell_2$  operation that can make the predictions only lie on the angle between the image feature and the identity prototype vectors. Finally, the visual features are distributed on a hypersphere with a radius of  $r$ . Here, the probability of the input image  $x$  belonging to the  $j$ -th prototype  $m_j$  can be represented as:

$$p(x \in m_j | x) = \frac{\exp^{r \cos \theta_j}}{\sum_{l=1}^N \exp^{r \cos \theta_l}} \quad (6)$$

where  $\theta_j$  represents the angle between  $v$  and  $m_j$ . Moreover, to enhance the intra-class compactness and the inter-class discrepancy, there adds an angular margin  $d$  penalty in the normalized hypersphere. Eq. (6) is then reformulated into:

$$p(x \in m_j | x) = \frac{\exp^{r \cos(\theta_j + q_j \cdot d)}}{\exp^{r \cos(\theta_y + d)} + \sum_{l=1, s_{il} \neq y}^N \exp^{r \cos \theta_l}} \quad (7)$$

where  $\theta_y$  represents the angle between  $v$  and the prototype with the same identity (i.e.,  $m_y$ ).  $q_j = 1$  if  $s_{ij} = y$  and 0 otherwise. Obviously, compared with the ranking loss based methods, the constraint of DCM in our MFHI can significantly enhance the inter-class separability. Unlike the previous triplet loss based methods [3] that consider only one positive pair and one negative pair, our DCM constraint constructs one positive pair and multiple negative pairs at the same time through prototype learning, which will be more conducive to insight into the distributions of different classes, and the separability between classes can be significantly enhanced. Finally, a promising model can be obtained by conducting a cross entropy loss as

$$\mathcal{L}_{\text{DCM}}(x, \hat{\mathbf{A}}_i^{tr}, y) = - \sum_{j=1}^N q_j \log p(x \in m_j | x). \quad (8)$$

#### F. MFHI: Recognition

For **I2A** and **A2I**, there exists a given testing set  $\{X^{te}, A^{te}, \hat{\mathbf{A}}^{te}\}$  with the unseen class set  $Y^u$ . Specially, for **I2A** scenario, to correctly classify any image sample in  $X^{te}$ , based on the category-level textual descriptions, the prototypes of all target identities covered in  $Y^u$  are first generated by the learned PLM. Then, the testing sample  $x^{te}$  is embedded into the shared space to obtain the visual feature  $v$ . After that,

the similarity scores between the visual feature  $v$  and every identity prototype are computed by cosine metric. Finally, the testing sample is classified to the nearest prototype. Let  $y^{te}$  denote the predicted label, which can be defined as:

$$y^{te} = \arg \max_{u_k \in Y^u} p(v \in m_k^{te} | x^{te}) \quad (9)$$

where  $m_k^{te} = \Phi(\hat{a}_k^{te})$  is the  $k$ -th target identity prototype and  $p(v \in m_k^{te} | x^{te}) = \frac{v^T \cdot m_k^{te}}{\|v\|_2 \|m_k^{te}\|_2}$ . Likewise, for **A2I**, the category-level attribute query is first fed into the PLM to produce the identity prototype. Afterwards, the visual feature of each image in the gallery set is obtained by the image embedding module. In the end, the similarity score between the identity prototype and each image feature is calculated by cosine metric. The gallery images with top rank scores are considered as the possible matches.

Different from the above two scenarios, there exist an image probe set  $X^q$  and an image gallery set  $X^{te}$  on **I2I**. Given an image query, we first obtain the visual features of the queried image and every gallery image, and meanwhile normalize them by  $\ell_2$  operation. Then, the pairwise similarity scores between the queried image feature and every gallery image feature are computed by Euclidean distance metric. Consequently, we treat the gallery images with top rank scores as the possible matches.

## IV. EXPERIMENTAL RESULTS AND ANALYSIS

In this section, we evaluate the proposed method on two challenging tasks, i.e., face identification and re-ID.

### A. Modality-Free Face Identification

**Datasets.** Among the most widely used datasets for face identification, we select two attribute datasets. (i) **CelebA** is a large scale face dataset that consists of 202,599 images about approximately 10k identities [29]. Each image is annotated with 40 binary attributes. (ii) **LFWA** [29] is created based on unconstrained face dataset LFW [30]. It contains 13,233 images of 5,749 identities, and each image is also labeled with 40 binary attributes.

**Protocols and Evaluation Metrics.** For CelebA dataset, we adopt the standard split in [29], with 162,770, 19,867, and 19,962 images for training, validation, and testing. For LFWA dataset, we divide it by randomly choosing identities, and construct training and testing sets at a ratio of 8:2. Specially, The training and testing identities are completely disjoint in two datasets. During the testing phase of **I2A** scenario, we treat a correct matching between the queried image and the gallery attribute description as a correct prediction. It is expected that our MFHI should have high performance on both densely and sparsely populated identities. Therefore, referring to [19], we select mean average per-class accuracy at Top-P as the metric where  $P \in \{1, 5, 10\}$ . For **A2I**, we treat the gallery images respecting a given attribute query as true matches. To evaluate the performance of MFHI, referring to [17], we use the Cumulative Match Characteristic (CMC) at R@P as the metric and we set  $P \in \{1, 5, 10\}$ .

TABLE II  
COMPARATIVE RESULTS (%) ON TWO DATASETS UNDER TWO SCENARIOS. RED/BLUE REPRESENT THE BEST/SECOND BEST RESULTS.

Method Categories	Datasets Methods	CelebA						LFWA					
		Image→Attribute			Attribute→Image			Image→Attribute			Attribute→Image		
		Top-1	Top-5	Top-10	R@1	R@5	R@10	Top-1	Top-5	Top-10	R@1	R@5	R@10
ZSL	DEM [6]	6.0	18.5	27.9	21.4	41.5	54.6	4.0	11.7	17.5	25.7	48.7	60.1
	RN [9]	0.5	2.5	5.0	0.1	2.2	4.1	0.5	1.1	1.8	0.2	0.6	1.1
	AREN [7]	24.3	51.5	63.8	3.6	10.6	14.9	21.9	47.2	59.9	1.3	4.1	6.6
GCL	VSE++ [26]	6.6	20.0	29.3	10.8	28.5	39.8	5.3	17.2	26.7	4.5	13.4	20.2
	VSRN [27]	9.5	25.5	35.2	16.9	38.0	49.9	7.4	21.0	30.5	6.4	18.3	27.2
LAL	SCAN [28]	4.7	14.6	21.8	6.4	18.9	28.5	4.6	11.7	16.6	2.6	9.0	14.0
	AttPre	15.2	34.4	46.3	20.5	45.9	57.0	21.7	41.5	53.1	26.3	51.6	62.5
GLL	MFHI	30.1	58.3	71.0	41.0	67.7	77.3	36.3	65.9	77.1	39.1	66.7	76.2

**Implementation Details.** For data preprocessing, we resize the face image to  $112 \times 112$ , and augment the training data with random flipping. The feature scale  $r$  is selected from  $\{32, 64\}$ , and the angular margin  $d$  is selected from  $\{0.1, 0.2, 0.3\}$ . For the visual embedding flow, we employ the widely used CNN in face recognition, IR-SE [31], and initialize it with the pretrained weight<sup>1</sup>. The output of the last convolutional layer with 512 channels is adopted as the visual feature map. Moreover, for the MLP of the identity prototype learning flow, the size of hidden layer is set to 256, and the output size is set to 512 that is the same as the visual feature dimension. In the spatial attention flow, the number  $D$  of attribute activation maps is set to 10, and the input size of attribute classifier is 512, while the output size is equal to the number of attributes. We select Adam optimizer where the learning rate is initialized to  $5e-5$  with the weight decay of  $5e-4$ .

**Compared Methods.** To evaluate the superiority of our joint global- and local-level (i.e., GLL) embedding approach, we compare with a wide range of plausible solutions to modality-free face identification problem. (i) *Global category-level visual-textual embedding* methods (i.e., GCL): Including two ZSL methods (i.e., DEM [6] and RN [9]) and two visual semantic embedding methods (i.e., VSE++ [26] and VSRN [27]). (ii) *Local attribute-level visual-textual embedding* methods (i.e., LAL): Such as a region proposal based dense image-text cross-modal matching method SCAN [28] and an attentive region embedding ZSL method AREN [7]. A method based on attribute prediction (named AttPre) is designed for face identification to evaluate the identification performance of relying on individual attribute recognition. For testing language models, including VSE++ [26], SCAN [28], and VSRN [27], we use random attribute sentences due to lack of order, and then report the average results for 10 trails. For all methods, we use IR-SE to extract visual features except SCAN [28] and VSRN [27], while SCAN [28] and VSRN [27] employ the pretrained bottom up attention model [32] as the visual embedding module. Moreover, it is worth noting that existing face identification methods cannot be extended to modality-free task, since they just consider a image modality.

**Experimental Results and Analysis.** We report the comparative results in Table II. It can be seen that: (i) Our MFHI outperforms all existing methods on two benchmarks in two scenarios, validating that our method is very flexible and can effectively address the modality-free face identification problem. For instance, for Top-1 of **I2A** and R@1 of **A2I**, the improvements obtained by our MFHI over the strongest

competitors on two datasets range from 5.78% to 19.60% and 12.84% to 14.43%, respectively. Such competitive results prove that the different face modalities (i.e., images and texts) possess the consistent distributions in the shared space by learning a semantic visual prototype for each identity. (ii) The state-of-the-art ZSL methods fail to excel due to higher inter-class similarity, larger intra-class variation, larger search spaces, and more challenging application scenarios. For example, the best ZSL method AREN [27] achieves satisfied results in **I2A**, but it significantly drops in **A2I**. (iii) Comparing with GCL methods and the LAL embedding method, we can find that there are larger improvements obtained by our MFHI. This indicates that these image-text matching methods which typically focus on point-to-point distribution consistency through paired image-text sample cannot effectively address the identification of unseen identities

### B. Modality-Free Person Re-Identification

**Datasets.** For re-ID, We select two representative person search datasets: Market-1501 dataset [33] and DukeMTMC-reID dataset [34], [14]. Market-1501 contains 751 identities for training and 750 identities for testing. The training set, gallery set, and probe set contain 12,936 images, 19,732 images, and 3,368 queried images respectively. Meanwhile, each image is annotated by 27 attributes. Both training and testing include 702 identities on DukeMTMC-reID. The training set, gallery set, and probe set contain 16,522 images, 17,661 images, and 2,228 queried images respectively. Meanwhile, each image is annotated by 23 attributes. In order to facilitate model training, we change the original attribute vector to the one-hot vector, and then the final dimension of the attribute vector is 35 for Market-1501 and 26 for DukeMTMC-reID. Specially, for **A2I** and **I2A** two scenarios, we re-assign semantic IDs for each person image according to its attribute vector rather than real identity, which means different people with the same attribute vector have the same semantic ID. Finally, for Market-1501, we have 508 semantic IDs for training and 484 semantic IDs for testing, and for DukeMTMC-reID, we have 300 semantic IDs for training and 387 semantic IDs for testing.

**Evaluation Metrics.** As the common setups [17], the gallery images respecting a given attribute/image query are considered as true matches in **A2I** and **I2I**. We also use the CMC at R@P and the mean Average Precision (mAP) [33] as our evaluation metrics, where  $P \in \{1, 5, 10\}$  in **A2I** and  $P \in \{1, 10\}$  in **I2I**. For **I2A**, we still use the mean average per-class accuracy at Top-P as the evaluation metric, where  $P \in \{1, 5, 10\}$

<sup>1</sup>[https://github.com/TreBlEn/InsightFace\\_Pytorch](https://github.com/TreBlEn/InsightFace_Pytorch)

TABLE III

COMPARATIVE RESULTS (%) ON MARKET-1501 DATASET AND DUKEMTMC-REID DATASET. - REPRESENTS THAT THESE METHODS DID NO RELEASE OFFICIAL CODES, AND RED/BLUE REPRESENT THE BEST/SECOND BEST RESULTS.

Method Categories	Datasets Methods	Market-1501							DukeMTMC-reID						
		Image→Attribute			Attribute→Image				Image→Attribute			Attribute→Image			
		Top-1	Top-5	Top-10	R@1	R@5	R@10	mAP	Top-1	Top-5	Top-10	R@1	R@5	R@10	mAP
ZSL	DEM [6]	22.6	48.9	59.1	34.0	48.1	57.5	17.0	10.7	28.2	38.6	22.7	43.9	54.5	12.9
	RN [9]	22.8	53.0	65.8	17.2	38.7	47.3	15.5	22.4	49.2	61.7	25.1	42.0	51.5	13.0
	AREN [7]	28.8	62.0	76.3	21.9	38.6	46.1	15.3	17.5	39.3	50.8	23.7	42.2	50.9	12.8
GCL	DeepCCA [35]	-	-	-	29.9	50.7	58.1	17.5	-	-	-	36.7	58.8	65.1	13.5
	2WayNet [36]	-	-	-	11.2	24.3	31.4	7.7	-	-	-	25.2	39.8	45.9	10.1
	MMD [37]	-	-	-	34.1	47.9	57.2	18.9	-	-	-	41.7	62.3	68.4	14.2
	DeepCoral [38]	-	-	-	46.1	61.0	68.1	17.1	-	-	-	46.1	61.0	68.1	17.1
	VSE++ [26]	15.3	38.7	51.3	27.0	49.1	58.2	17.2	7.9	21.8	31.1	33.6	54.7	62.8	15.5
	AAIPR [39]	-	-	-	40.2	49.2	58.6	20.6	-	-	-	46.6	59.6	69.0	15.6
LAL	VSRN [27]	8.2	27.8	41.6	11.6	30.3	41.5	7.2	10.4	28.1	38.5	25.2	57.4	69.4	14.0
	SCAN [28]	8.3	26.3	38.4	4.0	10.1	15.3	2.1	6.0	21.0	32.2	3.5	9.3	14.3	1.6
	GAN-RNN [40]	-	-	-	30.4	38.7	44.4	15.4	-	-	-	34.6	52.7	65.8	14.2
GLL	CMCE [41]	-	-	-	35.0	50.9	56.4	22.8	-	-	-	39.7	56.3	62.7	15.4
	AIHM [17]	-	-	-	43.3	56.7	64.5	24.3	-	-	-	50.5	65.2	75.3	17.4
	MFHI	36.2	68.2	80.0	44.8	66.9	74.4	33.5	27.5	59.2	71.6	57.9	76.1	81.9	31.8

TABLE IV

COMPARATIVE RESULTS (%) ON MARKET-1501 AND DUKEMTMC-REID DATASETS. - REPRESENTS THAT THESE METHODS DID NOT REPORT THE CORRESPONDING RESULTS, RR DENOTES RE-RANKING [42], AND RED/BLUE REPRESENT THE BEST/SECOND BEST RESULTS.

Methods	Market-1501			DukeMTMC-reID		
	R@1	R@10	mAP	R@1	R@10	mAP
PDC [43]	84.4	94.90	63.4	-	-	-
DPFL [44]	88.9	-	73.1	-	-	-
GLAD [45]	89.9	-	73.9	-	-	-
KPM(Resnet-50) [46]	90.1	97.9	75.3	80.3	-	63.2
PCB(Resnet-50) [47]	93.8	98.5	81.6	83.3	-	69.2
AANet(Resnet-50) [22]	93.9	98.6	82.5	86.4	-	72.6
MFHI(Resnet-50) [37]	95.1	98.9	88.6	90.9	96.8	80.6
GP-reID(Resnet-101)+RR [48]	93.0	-	90.0	89.4	-	85.6
SPReID(Resnet-152)+RR [49]	94.6	97.7	91.0	89.0	-	85.0
AANet(Resnet-152)+RR [22]	95.1	97.9	92.4	90.4	-	86.9
MFHI(Resnet-50)+RR	95.7	98.5	94.6	92.8	96.8	90.5

**Compared Methods.** For **A2I** and **I2A**, we compare our MFHI with several state-of-the-art person search methods by text attribute. These methods can be divided into three paradigms: *Global category-level* (i.e., GCL): Including CCA [35], [36], [38] and MMD [37] based cross-modal matching models, ZSL methods (i.e., DEM [6] and RN [9]), visual semantic embedding methods (i.e., VSE++ [26] and VSRN [27]) and GAN based visual-semantic alignment method (i.e., AAIPR [39]). *Local attribute-level* (i.e., LAL): Such as region proposal based matching method (i.e., SCAN [28]) and natural language query based person search (i.e., GAN-RNN [40] and CMCE [41]). *the combination of global- and local-level visual-textual embedding methods* (i.e., GLL): Including a visual-textual hierarchical embedding GLL method (i.e., AIHM [17]). Additionally, in order to evaluate the advantage of our MFHI on **I2I**, we compare with a wide range of competitive and representative image query methods.

**Implementation Details.** We resize the person image to  $256 \times 128$ . For data augmentation, we employ random flipping in **A2I** and **I2A**, and use random flipping and random erasing [50] in **I2I**. The feature scale  $r$  and the angular margin  $d$  are selected from  $\{8, 64, 128, 256\}$  and  $\{0.15, 0.2, 0.4\}$  respectively. For the visual embedding flow, we use the ResNet-50 model with instance normalization and batch normalization, which contains 2048 channels in the last convolutional layer. We initialize it with the pretrained weight<sup>2</sup>. Moreover, in the identity prototype learning flow, the hidden layer size of the MLP is set to 1024, and the input and output sizes are set to 35

and 2048 respectively. In the spatial attention flow, the number  $D$  of attribute activation maps is set to 8, the attribute classifier input size is 2048, and the output size is 35. Especially, we select Adam optimizer where the learning rate is initialized to  $5e-5$  with the weigh decay to  $5e-4$  in **I2A** and **A2I**, and the initial learning rate is set to  $5e-1$  in **I2I**.

**Experimental Results and Analysis.** The experimental results of re-ID are shown in Table III and Table IV, respectively. About the results, we have the following discussions.

From Table III, it can be observed that: (i) Our MFHI model outperforms a wide variety of state-of-the-art methods, e.g., over the second best method AREN [7] by a margin of 7.4% in Top-1 of **I2A** scenario on Market-1501, and over the strongest competitor person search model AIHM [17] by a margin of 7.4% (resp. 14.4%) in R@1 (resp. mAP) of **A2I** scenario on DukeMTMC-reID. (ii) By comparing with the hierarchical visual-textual embedding method AIHM [17], it can be found that capturing attribute-level discriminative regions is indeed essential for such a large-scale identification problem. (iii) The performance margins over the GCL methods and the LAL methods are more significant. Obviously, for such challenging large-scale tasks, modelling only from global perspective or local perspective is not the optimal solution. (iv) In addition, the state-of-the-art ZSL methods are hard to be extended to this problem because of its more categories, more complex background, and meaningless category names. In contrast, our MFHI can maximize the human identity separability by minimizing the distribution discrepancy between the modalities.

As shown in Table IV for **I2I**, we can find that: (i) MFHI model yields better performances than the state-of-the-art baselines whether re-ranking [42] is used or not. This validates that by performing a local spatial attention mechanism on visual data and maximizing the distribution consistency of identity prototypes and visual features, our MFHI effectively improves the discriminability of visual features. (ii) Comparing with AANet [22], which also use Resnet-50 as the visual embedding module, the improvements obtained by our MFHI over the best existing method are 1.2% (resp. 6.2%) in R@1 (resp. mAP) on Market-1501 dataset. (iii) We also compare MFHI with AANet (Res-152) [22] with re-ranking (i.e., +RR). Our MFHI achieves 0.6% and 2.22% significant improvements in R@1 and mAP on Market-1501 dataset, respectively, and meanwhile has lower complexity.

<sup>2</sup>https://github.com/Qidian213/Ranked\_Person\_ReID



Fig. 4. The visualization of class activation maps and the attribute attention map in face identification. We highlight the captured attentive region with a red rectangular frame in an activation map.

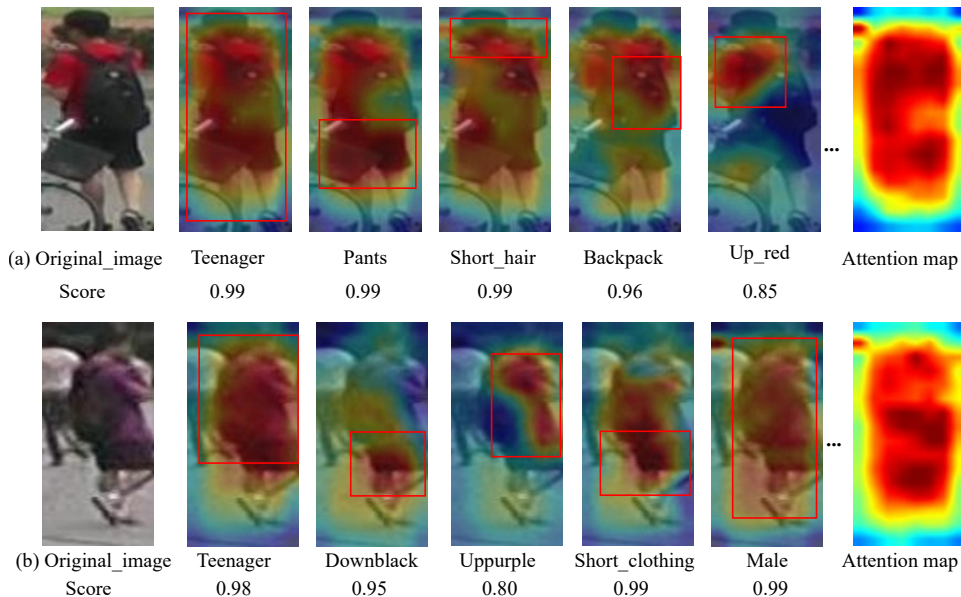


Fig. 5. The visualization of class activation maps and the attribute attention map in re-ID. We highlight the captured attentive region with a red rectangular frame in an activation map.

C. Qualitative Results Analysis

To provide more in-depth and visual evaluations for our MFHI, we design and conduct two qualitative discussions. First, as show in Fig. 4 and Fig. 5, we report the heatmaps of some discriminative attributes in face identification and re-ID, respectively. This can help us to analyze the effectiveness of semantics-guided spatial attention in MFHI. It can be found that: (i) Our method can accurately predict each individual attribute for four images of face identification and re-ID, so as to select the most significant local regions. (ii) In addition, Fig. 4 shows that the face attributes can be exactly localized in a face image by our method, like “bangs” in Fig. 4(a) and “black\_hair” in Fig. 4(b). Especially, for some local attributes that are difficult for people to observe, our model still can accurately capture the visual regions of these attributes, like “wearing\_lipstick” in Fig. 4(a) and “wearing\_earrings” in Fig. 4(b). (iii) As observed from Fig. 5, the wear appearance of the two people is successfully captured, like “backpack” in Fig. 5(a) and “uppurple” in Fig. 5(b). Then, by extracting such representative visual regions, the local-level discriminability of the visual features can be effectively enhanced. Finally, we can

obtain more reliable and interpretable identification.

Second, we show the examples of **A2I** on CelebA dataset and Market-1501 dataset, and **I2I** on Market-1501 dataset in Fig. 6. It can be seen that: (i) Most of the retrieval images exactly match the attribute query in Fig. 6(a) and Fig. 6(b). For example, MFHI accurately detects the local attributes (e.g., “eyeglasses” and “wavy\_hair”) as presented the R@1 image in Fig. 6(a). Meanwhile, we also find a false retrieval result due to the unobvious local attributes. For instance, it is hard to judge whether the R@4 image in Fig. 6(b) possesses “bags\_under\_eyes” attribute. (ii) In addition, as seen from the retrieval results in Fig. 6(d), due to the ambiguous visual appearance, there appear a few false retrieval results in re-ID. For example, the R@6 and R@10 images in Fig. 6(d) are “downblue”, while the R@4 image in Fig. 6(d) is “downblack”. (iii) For the common image queries, our MFHI obtains more outstanding performances as shown in Fig. 6(e) and Fig. 6(f). We can find that our MFHI correctly retrieves the target identity images in Fig. 6(e), while the false matches R@7 and R@8 images in Fig. 6(f) are due to very similar visual appearance of different identities.

TABLE V  
EFFECT OF LOCAL ATTRIBUTE-LEVEL DISCRIMINATION (%).

Datasets	CelebA						LFWA					
	Image→Attribute			Attribute→Image			Image→Attribute			Attribute→Image		
	Top-1	Top-5	Top-10	R@1	R@5	R@10	Top-1	Top-5	Top-10	R@1	R@5	R@10
GCL	22.8	49.9	63.3	32.4	59.5	69.0	33.6	63.4	74.6	32.1	56.6	67.4
MFHI	<b>30.1</b>	<b>58.3</b>	<b>71.0</b>	<b>41.0</b>	<b>67.7</b>	<b>77.3</b>	<b>36.3</b>	<b>65.9</b>	<b>77.1</b>	<b>39.1</b>	<b>66.7</b>	<b>76.2</b>

TABLE VI  
COMPARISONS TO THE SELF-ATTENTION ON PERSON RE-ID TASK(%).

Datasets	Market-1501							DukeMTMC-reID						
	Image→Attribute			Attribute→Image				Image→Attribute			Attribute→Image			
	Top-1	Top-5	Top-10	R@1	R@5	R@10	mAP	Top-1	Top-5	Top-10	R@1	R@5	R@10	mAP
Self-Attention [51]	26.5	59.4	72.4	37.1	63.2	71.7	32.6	24.7	54.5	67.7	50.3	73.2	81.1	28.8
MFHI	<b>36.2</b>	<b>68.2</b>	<b>80.0</b>	<b>44.8</b>	<b>66.9</b>	<b>74.3</b>	<b>33.5</b>	<b>27.0</b>	<b>58.8</b>	<b>71.5</b>	<b>57.2</b>	<b>74.1</b>	<b>81.2</b>	<b>31.5</b>



Fig. 6. The examples of **A2I** on CelebA dataset and Market-1501 dataset, and **I2I** on Market-1501 dataset. True or false images are indicated by green/red boxes respectively. We highlight the attributes in red corresponding to the false matches.

#### D. Ablation Study

**Effectiveness of Semantics-Guided Spatial Attention.** To evaluate the effectiveness of semantics-guided spatial attention in our MFHI, we examine two aspects of ablation study. On one hand, we remove the spatial attention flow in MFHI, and then just extract the visual features with global category-level (i.e., GCL) discrimination. The experimental results are reported in Table V. It can be concluded that: (i) Only global category-level discrimination is not sufficient to our tasks, although achieves higher performances than most compared methods. (ii) The improvements obtained by MFHI to GCL (2.5%~10.1% on LFWA dataset and 7.3%~8.6% on CelebA dataset) are significant. Obviously, learning category-level discrimination and capturing discriminative visual regions jointly is the optimal solution for modality-free human identification problem. Thus, local attribute-level discrimination with semantics-guided spatial attention is necessary.

On the other hand, to show the superiority of the proposed semantics-guided attention branch, we also replace the semantic attention in our MFHI by the popularly used self-attention

in [51] and conduct extensive experiments on person re-ID task. It can be seen from Tab. VI that our semantic-guided attention is better suited to such large scale identification tasks than self-attention. The main reason lies in that the self-attention mechanism is usually applied to capture long-range dependencies and has been shown to be effective in generating high-resolution image details. However, for such large scale identification tasks, the main challenge is to maximize the separability of human identity. Hence, a semantics-guided spatial attention is enforced on visual modality in our MFHI to enhance local-level discrimination.

#### E. Parameter Analysis

**Influence of the attribute activation map number (i.e.,  $D$ ).** As observed from Fig. 7, the number of attributes in an image obeys normal distribution on CelebA dataset, where  $\mu$  and  $\sigma$  represent its mean and standard deviation respectively. To explore the influence of  $D$  in our MFHI, we select a group of  $D$  by referring to the above statistics, and then conduct **I2A** and **A2I** experiments on CelebA dataset, where

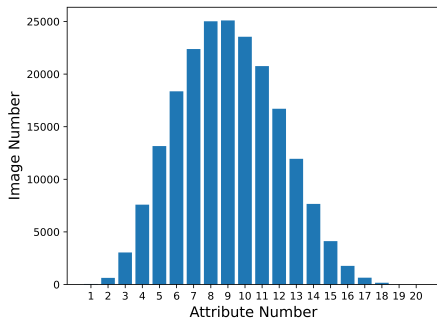


Fig. 7. The statistics of attributes on CelebA dataset.

TABLE VII  
THE INFLUENCE OF  $D$  ON OUR MFHI FOR CELEBA DATASET (%).

Value of $D$	Image→Attribute			Attribute→Image		
	Top-1	Top-5	Top-10	R@1	R@5	R@10
5	29.40	57.91	70.03	40.00	66.80	<b>77.30</b>
10	<b>30.09</b>	<b>58.25</b>	<b>70.98</b>	<b>41.00</b>	<b>67.70</b>	<b>77.30</b>
14	29.28	57.89	69.85	40.90	66.80	76.90

$D \in \{5, 10, 14\}$ . The comparative results are reported in Table VII. These results verify that: (i)  $D = 10$  (located on  $(\mu - \sigma, \mu + \sigma)$ ) outperforms other settings with an obvious margin (0.10%~1.13%), except in R@10 of **A2I**. (ii)  $D = 5$  and  $D = 14$  achieve unsatisfied performances, since the smaller number of attribute activation maps cannot capture enough representative local regions, while the larger number often brings noises, thus learning indiscriminate features.

**Influence of feature scale and margin (i.e.,  $r$  and  $d$ ).** For our MFHI, there still exist two parameters, i.e.,  $r$  and  $d$  in Eq. (7). By varying  $r$  from  $\{8, 16, 32, 64, 128\}$ ,  $d$  from  $\{0.1, 0.15, 0.2, 0.25, 0.3\}$ , and fixing other parameters as defaults, we run different models, and report both R@1 of **A2I** and Top-1 of **I2A** on LFWA dataset. In addition, we also conduct the same experiments on Market-1501 dataset to analyze the parameter influence on Top-1 and mAP. The experimental results are shown in Fig. 8, it can be observed that: (i) (64, 0.2) and (32, 0.3) are the optimal parameter settings for the two challenging scenarios **I2A** and **A2I** on LFWA dataset respectively. (ii) For Market-1501 dataset, (64, 0.2) performs best in the **I2A** scenario, while (8, 0.15) is more suitable for the **A2I** scenario. The above discussions further demonstrate that by selecting appropriate parameters, our MFHI can be flexibly applied to perform different tasks.

## V. CONCLUSION

We propose the first algorithmic framework for modality-free human identification task. In particular, we take an initial attempt, and formulate it as a generic zero-shot learning model. In addition, to maximize the human identity separability with interpretability, a semantics-guided spatial attention mechanism is enforced on visual modality. Furthermore, we bridge different modalities by learning a shared space, and then maximize their distribution consistency via learned identity prototypes. We have conducted extensive experiments on two challenging identification tasks, (i.e., face identification and re-ID), and achieve promising results compared with other alternatives. In essence, learning one prototype for an identity is generally insufficient to recognize one identity and differen-

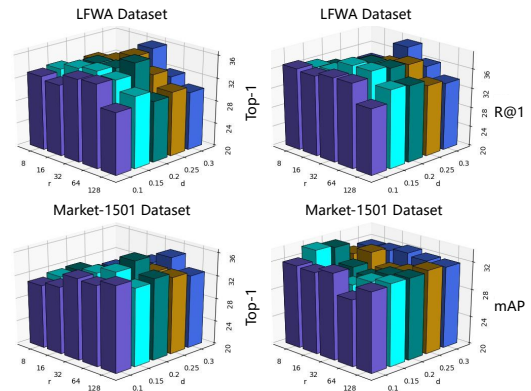


Fig. 8. The influence of  $(r, d)$  on LFWA dataset and Market-1501 dataset.

tiate two identities. Thus, our ongoing research work includes learning prototypes adaptively with the data distribution.

## REFERENCES

- [1] J. Deng, J. Guo, N. Xue, and S. Zafeiriou, “Arcface: Additive angular margin loss for deep face recognition,” in *Proc. CVPR*, 2019.
- [2] Z. Lai, Y. Xu, Z. Jin, and D. Zhang, “Human gait recognition via sparse discriminant projection learning,” *IEEE Transactions on Circuits and Systems for Video Technology*, vol. 24, no. 10, pp. 1651–1662, 2014.
- [3] K. Zeng, M. Ning, Y. Wang, and Y. Guo, “Hierarchical clustering with hard-batch triplet loss for person re-identification,” in *Proc. CVPR*, 2020.
- [4] K. G. Quach, P. Nguyen, H. Le, T.-D. Truong, C. N. Duong, M.-T. Tran, and K. Luu, “Dyglip: A dynamic graph model with link prediction for accurate multi-camera multiple object tracking,” in *Proc. CVPR*, 2021.
- [5] C. C. Loy, T. Xiang, and S. Gong, “Time-delayed correlation analysis for multi-camera activity understanding,” *International Journal of Computer Vision*, vol. 90, no. 1, pp. 106–129, 2010.
- [6] L. Zhang, T. Xiang, and S. Gong, “Learning a deep embedding model for zero-shot learning,” in *Proc. CVPR*, 2017.
- [7] G.-S. Xie, L. Liu, and et al, “Attentive region embedding network for zero-shot learning,” in *Proc. CVPR*, 2019.
- [8] Y. Annadani and S. Biswas, “Preserving semantic relations for zero-shot learning,” in *Proc. CVPR*, 2018.
- [9] F. Sung, Y. Yang, L. Zhang, and et al, “Learning to compare: Relation network for few-shot learning,” in *Proc. CVPR*, 2018.
- [10] H. Guo, K. Zhu, M. Tang, and J. Wang, “Two-level attention network with multi-grain ranking loss for vehicle re-identification,” *IEEE Transactions on Image Processing*, vol. 28, no. 9, pp. 4328–4338, 2019.
- [11] Q. Cao, L. Shen, W. Xie, O. M. Parkhi, and A. Zisserman, “Vggface2: A dataset for recognising faces across pose and age,” in *Proc. FG*, 2018.
- [12] F. Schroff, D. Kalenichenko, and J. Philbin, “Facenet: A unified embedding for face recognition and clustering,” in *Proc. CVPR*, 2015.
- [13] X. Xu, Y. Huang, P. Shen, and et al, “Consistent instance false positive improves fairness in face recognition,” in *Proc. CVPR*, 2021.
- [14] Y. Lin, L. Zheng, Z. Zheng, Y. Wu, Z. Hu, C. Yan, and Y. Yang, “Improving person re-identification by attribute and identity learning,” *Pattern Recognition*, vol. 95, pp. 151–161, 2019.
- [15] Z. Zheng, L. Zheng, M. Garrett, Y. Yang, M. Xu, and Y.-D. Shen, “Dual-path convolutional image-text embeddings with instance loss,” *ACM Transactions on Multimedia Computing, Communications, and Applications*, vol. 16, no. 2, pp. 1–23, 2020.
- [16] T. Chai, Z. Chen, A. Li, J. Chen, X. Mei, and Y. Wang, “Video person re-identification using attribute-enhanced features,” *arXiv preprint arXiv:2108.06946*, 2021.
- [17] Q. Dong, S. Gong, and X. Zhu, “Person search by text attribute query as zero-shot learning,” in *Proc. ICCV*, 2019.
- [18] X. Zhang, S. Gui, Z. Zhu, Y. Zhao, and J. Liu, “Hierarchical prototype learning for zero-shot recognition,” *IEEE Transactions on Multimedia*, vol. 22, no. 7, pp. 1692–1703, 2020.
- [19] Z. Liu, X. Zhang, Z. Zhu, S. Zheng, Y. Zhao, and J. Cheng, “Convolutional prototype learning for zero-shot recognition,” *Image and Vision Computing*, vol. 98, p. 103924, 2020.
- [20] S. Chen, W. Wang, B. Xia, and et al, “Free: Feature refinement for generalized zero-shot learning,” in *Proc. ICCV*, 2021.

- [21] S. Chen, G.-S. Xie, Y. Liu, Q. Peng, B. Sun, H. Li, X. You, and L. Shao, "Hsva: Hierarchical semantic-visual adaptation for zero-shot learning," *arXiv preprint arXiv:2109.15163*, 2021.
- [22] C.-P. Tay, S. Roy, and K.-H. Yap, "Aanet: Attribute attention network for person re-identifications," in *Proc. CVPR*, 2019.
- [23] F. Yang, R. Wang, and X. Chen, "Sega: Semantic guided attention on visual prototype for few-shot learning," *arXiv preprint arXiv:2111.04316*, 2021.
- [24] J. Ge, H. Xie, S. Min, and Y. Zhang, "Semantic-guided reinforced region embedding for generalized zero-shot learning," in *Proc. AAAI*, 2021.
- [25] B. Zhou, A. Khosla, A. Lapedriza, A. Oliva, and A. Torralba, "Learning deep features for discriminative localization," in *Proc. CVPR*, 2016.
- [26] F. Faghri, D. J. Fleet, J. R. Kiros, and S. Fidler, "Vse++: Improving visual-semantic embeddings with hard negatives," in *Proc. BMVC*, 2018.
- [27] K. Li, Y. Zhang, K. Li, Y. Li, and Y. Fu, "Visual semantic reasoning for image-text matching," in *Proc. ICCV*, 2019.
- [28] K.-H. Lee, X. Chen, G. Hua, H. Hu, and X. He, "Stacked cross attention for image-text matching," in *Proc. ECCV*, 2018.
- [29] Z. Liu, P. Luo, X. Wang, and X. Tang, "Deep learning face attributes in the wild," in *Proc. ICCV*, 2015.
- [30] G. B. Huang, M. Ramesh, T. Berg, and E. Learned-Miller, "Labeled faces in the wild: A database for studying face recognition in unconstrained environments," Tech. Rep. 07-49, 2007.
- [31] J. Hu, L. Shen, and G. Sun, "Squeeze-and-excitation networks," in *Proc. CVPR*, 2018.
- [32] P. Anderson, X. He, C. Buehler, D. Teney, M. Johnson, S. Gould, and L. Zhang, "Bottom-up and top-down attention for image captioning and visual question answering," in *Proc. CVPR*, 2018.
- [33] L. Zheng, L. Shen, L. Tian, S. Wang, J. Wang, and Q. Tian, "Scalable person re-identification: A benchmark," in *Proc. ICCV*, 2015.
- [34] E. Ristani, F. Solera, R. Zou, and et al, "Performance measures and a data set for multi-target, multi-camera tracking," in *Proc. ECCV*, 2016.
- [35] G. Andrew, R. Arora, J. Bilmes, and K. Livescu, "Deep canonical correlation analysis," in *Proc. ICML*, 2013.
- [36] A. Eisenschat and L. Wolf, "Linking image and text with 2-way nets," in *Proc. CVPR*, 2017.
- [37] I. O. Tolstikhin, B. K. Sriperumbudur, and et al, "Minimax estimation of maximum mean discrepancy with radial kernels," in *Proc. NIPS*, 2016.
- [38] B. Sun and K. Saenko, "Deep coral: Correlation alignment for deep domain adaptation," in *Proc. ECCV*, 2016.
- [39] Z. Yin, W.-S. Zheng, A. Wu, and et al, "Adversarial attribute-image person re-identification," in *Proc. IJCAI*, 2018.
- [40] S. Li, T. Xiao, H. Li, B. Zhou, D. Yue, and X. Wang, "Person search with natural language description," in *Proc. CVPR*, 2017.
- [41] S. Li, T. Xiao, H. Li, W. Yang, and X. Wang, "Identity-aware textual-visual matching with latent co-attention," in *Proc. ICCV*, 2017.
- [42] Z. Zhong, L. Zheng, D. Cao, and S. Li, "Re-ranking person re-identification with k-reciprocal encoding," in *Proc. CVPR*, 2017.
- [43] C. Su, J. Li, S. Zhang, J. Xing, W. Gao, and Q. Tian, "Pose-driven deep convolutional model for person re-identification," in *Proc. ICCV*, 2017.
- [44] Y. Chen, X. Zhu, and S. Gong, "Person re-identification by deep learning multi-scale representations," in *Proc. ICCVW*, 2017.
- [45] L. Wei, S. Zhang, H. Yao, W. Gao, and Q. Tian, "Glad: Global-local-alignment descriptor for scalable person re-identification," *IEEE Transactions on Multimedia*, vol. 21, no. 4, pp. 986-999, 2019.
- [46] Y. Shen, T. Xiao, H. Li, and et al, "End-to-end deep kronecker-product matching for person re-identification," in *Proc. CVPR*, 2018.
- [47] Y. Sun, L. Zheng, Y. Yang, Q. Tian, and S. Wang, "Beyond part models: Person retrieval with refined part pooling," in *Proc. ECCV*, 2018.
- [48] J. Almazán, B. Gajic, N. Murray, and D. Larlus, "Re-id done right: towards good practices for person re-identification," *arXiv preprint arXiv:1801.05339*, 2018.
- [49] M. M. Kalayeh, E. Basaran, M. Gokmen, and et al, "Human semantic parsing for person re-identification," in *Proc. CVPR*, 2018.
- [50] Z. Zhong, L. Zheng, G. Kang, S. Li, and Y. Yang, "Random erasing data augmentation," *arXiv preprint arXiv:1708.04896*, 2017.
- [51] H. Zhang, I. Goodfellow, D. Metaxas, and A. Odena, "Self-attention generative adversarial networks," in *Proc. ICML*, 2019.